Zero-Reconvergence PPP for Real-Time Low-Earth Satellite Orbit Determination in Case of Data Interruption

Haibo Ge, Guanlong Meng, and Bofeng Li

***Abstract*—With the fast development of low earth orbit (LEO) enhanced global navigation satellite system (LeGNSS), there is huge demand in LEO real-time precise orbit determination. Real-time service from international GNSS service (IGS) provides the real-time precise GNSS orbit and clock products, which gives an opportunity to make use of kinematic precise point positioning (PPP) method for LEO POD. However, real-time precise GNSS products and onboard GNSS observations interrupt inevitably or even frequently (especially for real-time clock products), resulting in PPP reconvergence as well as large orbit errors in LEO orbit solutions. A new method is put forward to reduce such influence of two types of data interruptions. For interruption of clock products, the Chebyshev extrapolation is used to maintain the continuity of real-time GNSS clock products. For the onboard observation interruption, the predicted dynamic orbits are employed as constraints to overcome the PPP reconvergence. Results show that zero-reconvergence PPP can be realized with our new method, which means there is almost no reconvergence time after data interruption. Moreover, clock prediction can reduce the root–mean-square errors (RMSE) for real-time LEO orbit from 5.40, 4.70, and 7.33 cm to 5.18, 4.55, and 5.99 cm in along-track, cross-track, and radial directions, respectively, while the predicted dynamic orbit constraints reduce the orbit RMSE by 20–30% in cross-track component and 60%–80% in other two components.**

***Index Terms*—Data interruption, low earth orbit (LEO) satellites, precise point positioning (PPP) reconvergence, real-time kinematic orbit determination.**

I. Introduction

PRECISE low earth orbits (LEO) are the prerequisite for the geoscientific research and applications with different kinds of LEO satellites, such as earth gravimetry [1], ocean tides [2], and earth magnetic field [3]. Two typical methods are commonly used to determine the precise orbits of LEO satellites, e.g., kinematic precise orbit determination (KPOD) [4] and reduced-dynamic precise orbit determination (RDPOD) [5]. KPOD only uses pseudo-range and carrier phase observations received by onboard GNSS receivers. It is clear that the orbit accuracy of KPOD mainly depends on the GNSS satellite geometry and the observation quality since the dynamic force model is not adopted. Combining GNSS observations and dynamic force models, RDPOD can obtain the precise LEO satellite orbits with 1–2 cm accuracy [6], where the process noise or empirical parameters should be properly set up to absorb the unmodeled errors in dynamic force models. For some specific research and applications, such as gravity recovery, KPOD is preferred since it is not affected by force models. Moreover, KPOD is much more computationally efficient than RDPOD, which is more suitable for the upcoming mega LEO constellations with the huge number of satellites [7].

KPOD is generally implemented by precise point positioning (PPP) method [8], [9]. Montenbruck [10] demonstrated that the total root-mean-square errors (RMSE) of CHAMP are about 1.0–1.5 m with 30 s sampling data by using single frequency PPP. With the improvement of GPS precise products as well as the adoption of dual-frequency data, the RMSE of kinematic orbits for each direction can be smaller than 2.5 cm for GRACE, CHAMP, and GOCE satellites [11], [12], [13].

In recent years, with huge demand of real-time positioning services and different kinds of real-time applications, especially for the real-time PPP of LEO enhanced global navigation satellite systems (LeGNSS) [14], real-time precise LEO orbits have become one of the research hotspots. Meanwhile, with the launch of real-time service (RTS) [15] and the refinement of models and strategies for GNSS POD, the accuracy of real-time GNSS orbit and clock generated by International GNSS Service (IGS) has been improved greatly. The accuracy of real-time GPS orbits reaches centimeter level and the standard deviations (STD) of GPS clock is about 0.1 ns, providing the centimeter level real-time positioning accuracy [16], [17]. The improvement of IGS-RTS gives opportunities for real-time precise LEO orbit determination with real-time PPP. Real-time decimeter LEO orbit can be obtained with single-frequency GPS data while it can be improved to centimeter-level with double-frequency data, such as sentinel-3A and swarm-A [18], [19]. With the increasing

Manuscript received 24 July 2023; revised 13 October 2023; accepted 1 February 2024. Date of publication 6 February 2024; date of current version 20 February 2024. This work was supported in part by the National Natural Science Funds of China under Grant 42104013, Grant 42225401, Grant 42074026), in part by the Fundamental Research Funds for the Central Universities, in part by the Natural Science Funds of Shanghai under Grant 21ZR1465600, in part by the Innovation Program of Shanghai Municipal Education Commission under Grant 2021-01-07-00-07-E00095, in part by the Program of Shanghai Academic Research Leader under Grant 20XD1423800, in part by the "Shuguang Program" supported by Shanghai Education Development Foundation and Shanghai Municipal Education Commission under Grant 20SG18, and in part by the Scientific and Technological Innovation Plan from Shanghai Science and Technology Committee under Grant 21511103902 and Grant 22511103003. *(Corresponding author: Bofeng Li.)*

The authors are with the College of Surveying and Geo-Informatics, Tongji University, Shanghai 200092, China (e-mail: haibo_ge@tongji.edu.cn; 2231968@tongji.edu.cn; bofeng_li@tongji.edu.cn).

Digital Object Identifier 10.1109/JSTARS.2024.3362395

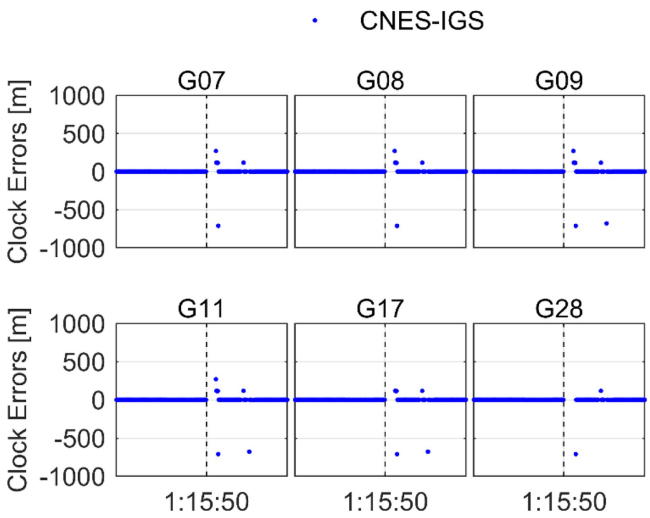

Fig. 1. Differences between CNES real-time clock and IGS final clock of G07, G08, G09, G11, G17, and G28 on January 10, 2019. Black dash line denotes the time when clock interruption occurs.

number of LEO satellites as well as the requirement of real-time precise LEO orbits, more studies on LEO real-time kinematic orbit determination are carried out and centimeter-level accuracy is achievable [20], [21], [22].

However, the interruption of real-time GNSS precise products and LEO onboard GNSS observations was neglected for the aforementioned studies, which would result in PPP reconvergence and greatly decrease the quality of real-time LEO orbit. Due to network outage or temporary modem failure, RTS products may interrupt frequently, especially for real-time clock [23], [24]. The influence of real-time clock outage for the ground real-time PPP has been investigated thoroughly and the corresponding prediction models have been well studied, such as linear model, polynomial model, and grey model [25], [26], [27], while the impact of such interruptions on real time LEO orbit determination is rarely investigated. In addition, the stream of GNSS real-time clock also jumps frequently, which may be caused by the switchover of clock datum [28]. For ground stations, clock detection and prediction methods for removing clock jumps has been studied and achieved great improvements in real-time positioning [24], [29]. Nevertheless, the impact of real-time GNSS clock interruption and jump on real-time LEO orbit determination are rarely assessed. Furthermore, the performance of onboard GNSS receiver could be impaired [30] and onboard GNSS observations may interrupt as well due to the complex space environment [31], [32]. Under such circumstance, real-time LEO orbits are unavailable since the lack of onboard observations. Moreover, real-time PPP of LEO orbit would suffer from reconvergence when onboard observation data recovered. For ground stations, tropospheric and ionospheric constraints are usually adopted for the fast PPP reconvergence in real-time [33], [34]. However, they are not suitable for the LEO satellites, since the altitude of LEO orbit is higher than that of troposphere and the real-time maps or products for topside ionosphere of LEO are not provided. Thus, the precision of real-time LEO orbit would decrease to decimeter-level or even meter-level during the reconvergence period, which is unacceptable for the real-time precise applications.

In this article, we put forward the method of zero-reconvergence PPP for real-time LEO orbit determination in case of data interruption. For the interruption of onboard observation data, constraining the predicted orbit for kinematic orbit determination is proposed in order to accelerate the speed of reconvergence or even avoid the reconvergence. For the interruption of real-time GNSS clock, a clock jump detection method is put forward and Chebyshev extrapolation is then adopted to predict real-time clock to improve the quality of LEO orbit during real-time clock interruption.

The rest of this article is organized as follows. In Section II, datasets and the phenomenon of real-time clock and onboard data interruptions are demonstrated in the following section. In Section III, the corresponding PPP solutions for LEO orbit determination are introduced. In Section IV, the performance and analysis of new strategies are given. Finally, Section V concludes this article.

II. Demonstration of Datasets

Data of gravity recovery and climate experiment follow-on (GRACE-FO) from January 1–30, 2019, e.g., onboard GPS data (GPS1B), attitude data (SCA1B), and precise scientific orbits (GNV1B) are adopted to perform real-time KPOD. GPS1B data contains dual-frequency GPS observations of the twin satellites, GRACE-C and GRACE-D, with sampling interval of 10 s. SCA1B data contains the rotation quaternions from inertial frame to satellite frame [35]. GNV1B data is precise scientific orbits of GRACE-FO generated by RDPOD of Jet Propulsion Laboratory (JPL), which has been widely used as reference orbit due to its high accuracy. All the datasets above are accessible via Physical Oceanography Distributed Active Archive Center website (https://podaac-tools.jpl.nasa.gov/drive/files/allData/). Meanwhile, real-time GNSS orbits and clock corrections from Centre National D'Etudes Spatiales (CNES) are used, which can be found in the website: http://www.ppp-wizard.net/products/REAL_TIME/.

Fig. 1 shows the clock differences between real-time clock products from CNES and final clock products from IGS of G07, G08, G09, G11, G17, and G28 for half an hour on January 10, 2019. It can be found that the real-time clocks interrupt for about two minutes from 1:15:50 to about 1:18. Moreover, large differences exist between CNES real-time clock products and IGS products and the maximum deviation can reach over 700 m.

Fig. 2 shows the statistic results of clock interruption durations for each GPS satellite in January 2019 (G04 is not included since there is no real-time products for it). It is clear that almost all satellites have 10 times of clock interruptions for 1 min, while G18 and G27 have nearly 15 times of clock interruptions. Moreover, the periods of clock interruption are all within 6 minutes.

Meanwhile, the interruption of onboard GNSS observations is also found in the datasets. Fig. 3 shows the observed number of GPS satellites of GRACE-D on January 26, 2019. Clearly,

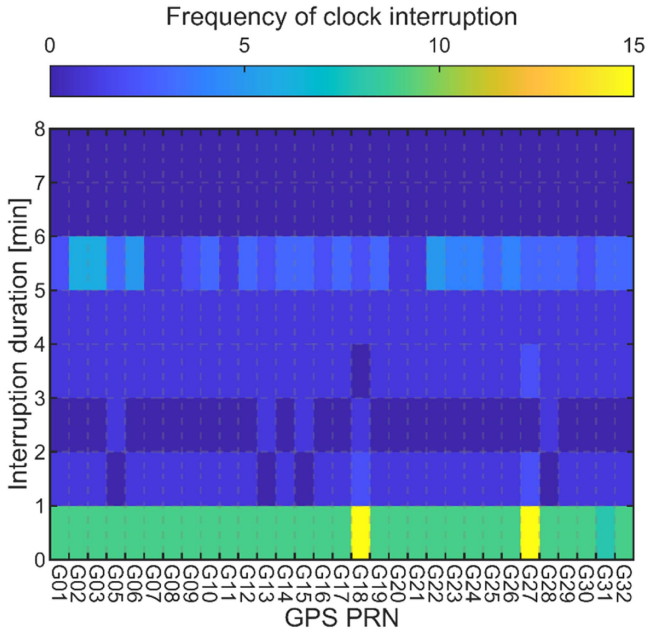

Fig. 2. Frequency and duration of clock interruptions for each GPS satellite in January, 2019. The vertical axis represents the interruption duration for each GPS satellite, and the color indicates the corresponding frequency for each interruption duration.

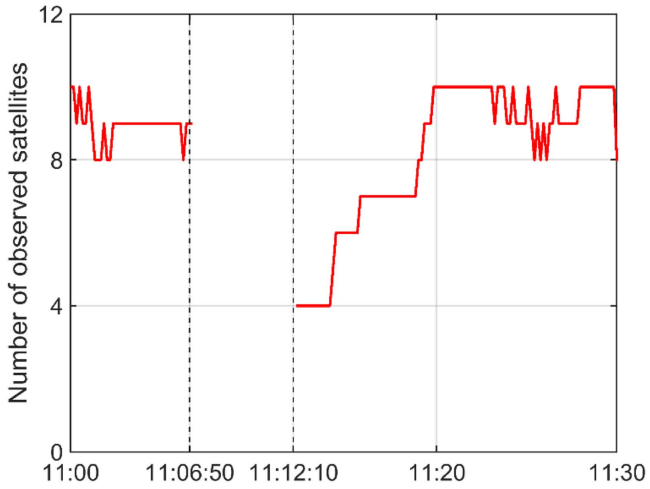

Fig. 3. Number of observed satellites by GRACE-D on January 26, 2019. Black dash lines denote the period of observation interruption (from 11:06:50 to 11:12:10).

the observation interruption starts at 11:06:50 and recovers at 11:12:10, with a duration of approximately 5 min.

In order to find out the length of onboard observation interruption, all onboard observations of GRACE-FO in 2019 are used for statistical analysis. Fig. 4 shows the statistical results of different interruption periods for GRACE-C and GRACE-D in 2019. As shown in Fig. 4, the lengths of most onboard observation interruptions are 4–6 min for GRACE-C and GRACE-D, while the longest interruption period is about 10 min for GRACE-C and about 9 min for GRACE-D. Moreover,

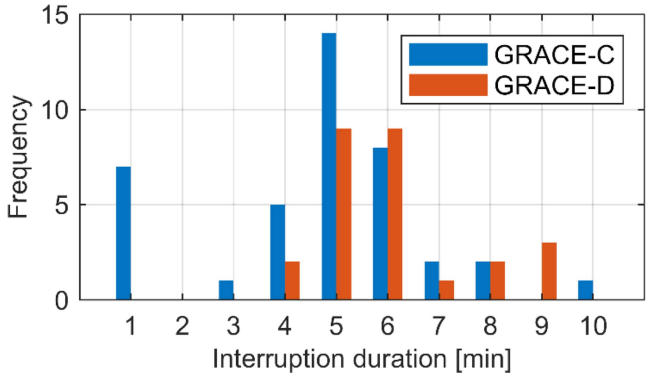

Fig. 4. Frequency as a function of interruption duration for GRACE-C (blue) and GRACE-D (red) observation data interruption in 2019.

the number of interruptions of GRACE-C is more than that of GRACE-D in 2019.

III. Processing Strategy

The aforementioned demonstrates that the interruptions or jumps of real-time clock products and onboard observation data are inevitable. If such interruptions or jumps are neglected in PPP processing, LEO orbit must reconverge once the data is recovered, resulting in great degradation of LEO orbit accuracy. Thus, it is of great importance to deal with these two types of interruptions to speed up or even avoid the PPP reconvergence and then keep the precision of LEO orbit stable. In this section, two strategies are put forward to alleviate the effects of clock and observation interruptions.

A. Setup of Real-Time PPP for LEO Satellites

We develop a real-time LEO orbit determination software based on the multisystem and multifrequency instantaneous precise point positioning [36]. The related processing setups are given in Table I. Ionosphere-free combination is applied to eliminate the impact of the ionospheric delay. Meanwhile, real-time PPP are carried out by the Kalman Filter. The IGS antenna file IGS14.atx is applied to correct the GPS PCO and PCV [37]. The PCO values of GRACE-FO are corrected by using SCA1B and VGN1B products [38].

B. Strategy of Real-Time Clock Interruption and Jump

The period of clock interruptions is mainly shorter than 6 minutes, c.f. Fig. 2. Nie et al. [29] summarized that the outage periods of real-time clock were mainly shorter than 3 min. Thus, many prediction models for clock corrections, e.g., neural network, grey model, Chebyshev extrapolation, and polynomial model etc., can be applied since the quality of short-term clock prediction (CP) is of high accuracy [40], [41]. Liu et al. [42] and Wang [43] predicted GPS clock with Chebyshev extrapolation, which can be expressed as

$$\delta t^{s}\ (t) = \sum_{i=0}^{n} C_i T_i\,(\tau) \tag{1}$$

TABLE I
MEASUREMENTS AND PROCESSING MODELS

ITEMS	MODELS
GPS MEASUREMENTS	
Basic observations	Undifferenced Ionosphere-free Code and Phase
GPS orbits and clocks	CNES real-time products
Stochastic model	Elevation Dependent Model
Sampling rate	10 s
Elevation cutoff	5°
GPS PCO/PCV	IGS14.atx [37]
GRACE-FO PCO	SCA1B and VGN1B [38]
Phase windup	Corrected [39]
Ionosphere delay	Ionosphere-free Combination
Relativity effect	Post-Newtonian correction
Estimation	
Processing mode	Kalman Filter
Estimation parameters	LEO satellite positions (epoch-wise estimated); Receiver clock offsets (epoch-wise estimated as white noise); Phase ambiguities (estimated as constant)

where $\delta t^s(t)$ is the satellite clock at time t; n is the Chebyshev order and C_i is the ith Chebyshev coefficient to be estimated. $\tau = 2(t-t_0)/\Delta t - 1$ donates the standardized time that ranges from -1 to 1 when fitting satellite clock. t_0 and Δt are the initial time and fitting duration, respectively. The recurrence formula $T_i(\tau)$ is formed as follows:

$$\begin{cases} T_0(\tau) = 1 \\ T_1(\tau) = \tau \\ T_n(\tau) = 2\tau T_{n-1}(\tau) - T_{n-2}(\tau),\ |\tau| \le 1,\ n \ge 2 \end{cases}. \quad (2)$$

Combining (1) and (2), the error equation is expressed as

$$\underbrace{\begin{bmatrix} V_1 \\ V_2 \\ \vdots \\ V_m \end{bmatrix}}_{\boldsymbol{V}} = \underbrace{\begin{bmatrix} T_0(\tau_1) & T_1(\tau_1) & \cdots & T_n(\tau_1) \\ T_0(\tau_2) & T_1(\tau_2) & \cdots & T_n(\tau_2) \\ \vdots & \vdots & \ddots & \vdots \\ T_0(\tau_m) & T_1(\tau_m) & \cdots & T_n(\tau_m) \end{bmatrix}}_{\boldsymbol{A}} \times \underbrace{\begin{bmatrix} C_0 \\ C_1 \\ \vdots \\ C_n \end{bmatrix}}_{\boldsymbol{X}} - \underbrace{\begin{bmatrix} \delta t^s(t_1) \\ \delta t^s(t_2) \\ \vdots \\ \delta t^s(t_m) \end{bmatrix}}_{\boldsymbol{l}} \quad (3)$$

where the Chebyshev coefficients are estimated by the least squares $\boldsymbol{X} = (\boldsymbol{A}^T\boldsymbol{A})^{-1}(\boldsymbol{A}^T\boldsymbol{l})$. With Chebyshev coefficients, the satellite clock can be predicted by the time t.

Besides clock interruptions, clock jumps shown in Fig. 1 must be detected and repaired, otherwise the results of LEO orbit would degrade greatly. The change rate of clock corrections is introduced as the detection index to find out clock jumps in real-time, which can be written as follows [24], [29]:

$$r_{\text{clk}} = \frac{clk_i - clk_{i-1}}{t_i - t_{i-1}} \quad (4)$$

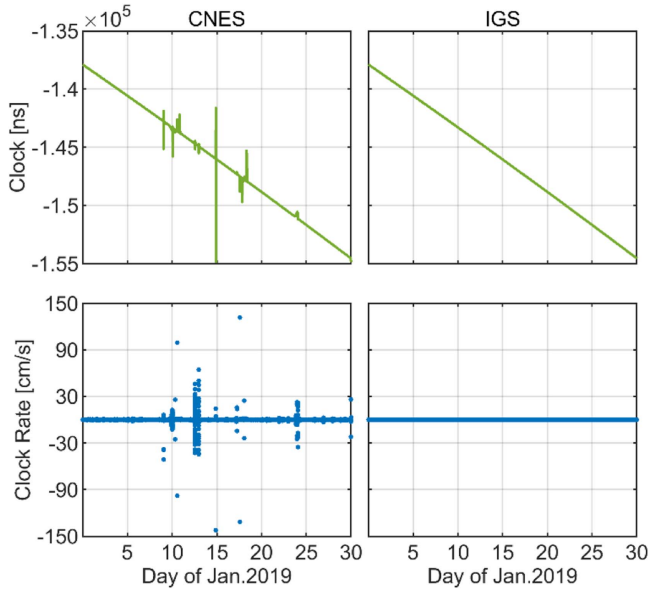

Fig. 5. Original clock corrections (top) and change rates (bottom) of G01 from CNES real-time products and IGS final products in January, 2019.

where clk_i and clk_{i-1} are corresponding GPS satellite clock corrections for epoch t_i and t_{i-1}, respectively. Fig. 5 shows the original clock corrections and change rates of G01 from CNES real-time products and IGS final products in January 2019. Both clock corrections exhibit a linear trend, while clock jumps occur occasionally for CNES real-time products. Moreover, real-time clock rate concentrates between -30 and 30 cm/s, while that of IGS final clock is steady and closed to zero.

Fig. 6 shows the STD of change rates of real-time clock for each GPS satellite in January 2019. The STD of clock change rates is about 7 cm/s for most satellites, while it is 3.37 cm/s for G18 and 4.30 cm/s for G31.

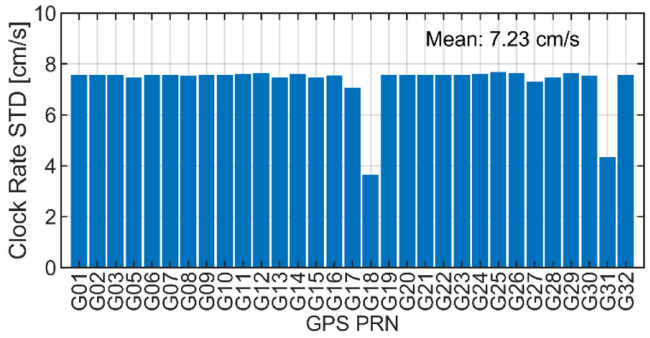

Fig. 6. STD of real-time clock change rate for each GPS satellite based on the data of January 1–30, 2019. Averaged value is in the upper right corner of this figure.

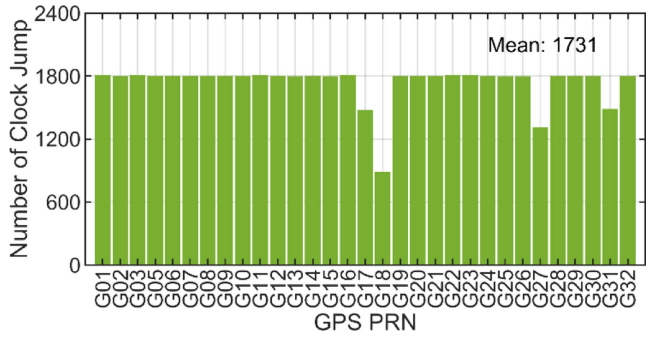

Fig. 7. Number of real-time clock jumps for each GPS satellite based on the data of January 1–30, 2019. Averaged number of jumps is in the upper right corner of this figure.

The three times STD is applied as a threshold for clock change rate to detect clock jump in real-time [24], [29], the number of detecting clock jumps for each satellite are shown in Fig. 7. The average number of clock jumps is about 1731 in January 2019. The amount of clock jumps for all satellites except G17, G18, G27, and G31 are similar about 1800, which may be caused by the switch of clock datum. When clock datum switches, clock offsets of different satellites jump at the same time, leading to the similar number of clock jumps [24]. However, the number of clock jumps for G17, G18, G27, and G31 is less than 1800, which is mainly caused by the interruption of clock products when the change of clock datum occurs, resulting in less detected clock jumps. When clock jumps are detected in real-time, CP is adopted and the jumps are replaced by the values predicted by Chebyshev extrapolation for LEO orbit determination.

C. Strategy of Onboard Observation Interruption

Kalman Filter is employed to implement the real-time PPP as follows [44], [45]:

$$\begin{cases} \boldsymbol{K}_k = \boldsymbol{P}_k^- \boldsymbol{H}^{\mathrm{T}} \left(\boldsymbol{H} \boldsymbol{P}_k^- \boldsymbol{H}^{\mathrm{T}} + \boldsymbol{R} \right)^{-1} \\ \hat{\boldsymbol{X}}_k = \hat{\boldsymbol{X}}_k^- + \boldsymbol{K}_k \left(\boldsymbol{Z}_k - \boldsymbol{H} \hat{\boldsymbol{X}}_k^- \right) \\ \boldsymbol{P}_k = (\boldsymbol{I} - \boldsymbol{K}_k \boldsymbol{H}) \ \boldsymbol{P}_k^- \end{cases} \tag{5}$$

where $\boldsymbol{K}_k$ is the Kalman Gain; $\boldsymbol{P}_k^-$ and $\boldsymbol{P}_k$ are the covariance matrix of state vector before and after measurement update; $\boldsymbol{H}$ is the state-to-measurement matrix; $\boldsymbol{R}$ is covariance matrix of GNSS measurement; $\boldsymbol{Z}_k$ is the GNSS measurement; $\hat{\boldsymbol{X}}_k^-$ and $\hat{\boldsymbol{X}}_k$ are the parameters before and after being filtered. Before measurement update, variances of LEO positions and receiver clock in $\boldsymbol{P}_k^-$ are set to a sufficient large number [in the article, we take $(60\ \mathrm{m})^2$] to handle them as purely epoch-wise parameters. Meanwhile, their corresponding values in $\hat{\boldsymbol{X}}_k^-$ are determined by the standard point positioning. The covariance matrix $\boldsymbol{R}$ is designed by the elevation dependent model and the state-to-measurement matrix $\boldsymbol{H}$ is generated by linearizing the code and phase observation equations. Updating measurement with the above matrices, real-time LEO orbits are obtained with a high accuracy.

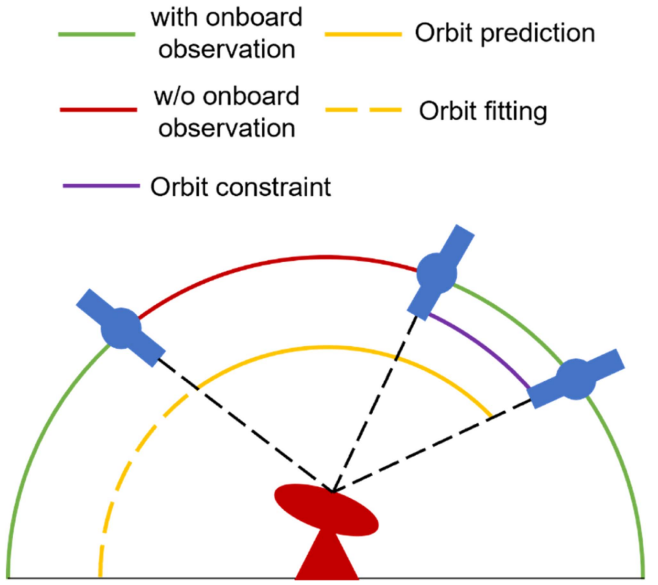

Fig. 8. Process of accelerating convergence based on predicting LEO orbit by dynamic force models. The green arcs represent normal conditions (with onboard observation), and the red arc indicates observation interruption (without (w/o) onboard observation). LEO orbit is fitted (yellow dashed arc) and predicted (yellow solid arc) when observation interrupt, and the prediction part is used as OC (purple arc).

However, onboard observation interruption will lead to the reconvergence of real-time kinematic PPP for POD, degrading the accuracy of real-time LEO orbits. Therefore, an orbit constrained method is proposed to avoid the reconvergence after onboard observation recovered. The basic concept is demonstrated in Fig. 8. When onboard observation interrupts, the kinematic orbits before interruption are used to predict the orbits. After data recovery, the predicted orbits are used as prior orbits and the precision of predicted orbits is used as prior constraints to accelerate PPP reconvergence. Therefore, the accuracy of orbit prediction is of great importance for PPP reconvergence. Due to fast motion and complicated perturbing dynamic forces of LEO satellites, the prediction accuracy of simple extrapolation methods, such as Chebyshev polynomial and Lagrange polynomial, would be larger than 1 m when prediction arc is longer than 1 min [46]. Predicting LEO orbits by using dynamic force models would reach higher accuracy [47], [48]. Wang et al. [49]

TABLE II
FORCE MODELS AND ESTIMATED PARAMETERS

ITEMS	MODELS/DESCRIPTION
Force models	
Gravity model	EIGEN-6C (120×120) [51]
Solid earth tide	IERS 2010 [52]
Ocean tide	Empirical ocean tide model EOT11A [53]
Solar radiation	Macro model [54]
Atmosphere drag	DTM94 [55]
N-body	JPL Planetary Ephemeris DE405 [56]
Parameters	
LEO orbits	Initial positions and velocities
Atmosphere drag	A scale factor estimated per resolution (90 min)
Empirical force	Ca, Sa, Cc, and Sc for along-track and cross-track components (cosine/sine) estimated per revolution

demonstrated that the orbital prediction accuracy can reach 0.1 m even for 1 h prediction arc. Thus, we use dynamic force models to fit and predict real-time LEO orbits.

The position $\boldsymbol{r}$ of satellite at t in dynamic model can be calculated as follows [50]:

$$\boldsymbol{r} = \boldsymbol{\Phi}(t, t_0)\left[\boldsymbol{r}_0, \dot{\boldsymbol{r}}_0, \boldsymbol{p}_0\right]^T \tag{6}$$

where $\boldsymbol{r}_0$, $\dot{\boldsymbol{r}}_0$, $\boldsymbol{p}_0$ represent the initial position, velocity, and dynamical parameters, respectively at t_0. $\boldsymbol{\Phi}(t, t_0) = \left[\partial \boldsymbol{r}/\partial \boldsymbol{r}_0 \quad \partial \boldsymbol{r}/\partial \dot{\boldsymbol{r}}_0 \quad \partial \dot{\boldsymbol{r}}_0/\partial \boldsymbol{p}_0\right]$ is the transform matrix of the orbit status from t_0 to t, which is calculated by orbit integration base on force models. Utilizing real-time kinematic LEO orbit within (t_1, t_n) to fit the initial orbit status can be expressed as the following form:

$$\begin{bmatrix} \boldsymbol{r}_{t_1} - \boldsymbol{r}^0_{t_1} \\ \boldsymbol{r}_{t_2} - \boldsymbol{r}^0_{t_2} \\ \vdots \\ \boldsymbol{r}_n - \boldsymbol{r}^0_{t_n} \end{bmatrix} = \begin{bmatrix} \boldsymbol{\Phi}(t_1, t_0)\left[\boldsymbol{\Delta r}_0, \boldsymbol{\Delta \dot{r}}_0, \boldsymbol{\Delta p}_0\right]^T \\ \boldsymbol{\Phi}(t_2, t_0)\left[\boldsymbol{\Delta r}_0, \boldsymbol{\Delta \dot{r}}_0, \boldsymbol{\Delta p}_0\right]^T \\ \vdots \\ \boldsymbol{\Phi}(t_n, t_0)\left[\boldsymbol{\Delta r}_0, \boldsymbol{\Delta \dot{r}}_0, \boldsymbol{\Delta p}_0\right]^T \end{bmatrix} \tag{7}$$

where $r^0_{t_i}$ is the kinematic LEO position, and r_{t_1} is calculated by orbit integration at t_i; $(\Delta \boldsymbol{r}_0, \Delta \dot{\boldsymbol{r}}_0, \Delta \boldsymbol{p}_0)$ are the corrections vectors of position, velocity and estimated dynamical parameters at t_0, respectively; $\boldsymbol{\Phi}(t_i, t_0)$ is the transform matrix from t_0 to t_i.

According to (7), the LEO position, velocity, and dynamic parameters at the initial time t_0 are estimated by using the iterative least squares estimation. Then, LEO orbits are predicted by using the numerical integration. The force models and the estimated parameters are given in Table II.

After observations recover, the prediction orbit is adopted as prior orbit, which is $\hat{X}_k^-$ in (5). Then, the corresponding position variances, P_k^- in (5), are set by the accuracy of prediction as a constraint. By constraining LEO orbit, the reconvergence can be accelerated. However, the accuracy of prediction orbit is unavailable in real-time since the reference orbit are usually postprocessed. Thus, an empirical accuracy of the predicted orbit needs to be determined.

In order to find out the appropriate constraint for predicted LEO orbits, total of 30-day real-time kinematic orbits are used to evaluate the accuracy of predicted orbits. Fig. 9 shows the averaged RMSE for 30 days in along-track, cross-track, and radial directions within 30 min. It is found that the prediction RMSE are smaller than 10 and 20 cm for 30-min prediction arc for the cross-track and radial direction, respectively. The prediction RMSE at along-track direction increases quickly as increasing the prediction arc and it is larger than 40 cm for 30-min prediction arc. The 3-D RMSEs of predicted orbits are 13.4, 18.7, and 25.1 cm for the prediction arc of 5, 10, and 15 min, respectively.

With the analysis above, the specific strategy used in our software for real-time kinematic PPP for LEO orbit determination when interruption of onboard data occurs is demonstrated as follow. During the period of interruption of onboard observation data, the initial parameters for orbit prediction are estimated with previous orbits. Then, the predicted orbits are used for orbit constraints (OC) after onboard observation recovered. In (5), the LEO positions in $\hat{\boldsymbol{X}}_k^-$ before measurement update are replaced by predicted orbit and the corresponding variances in $\boldsymbol{P}_k^-$, variances of position parameters, are replaced with the empirical accuracy. As shown in Fig. 9, the prediction errors in the three directions are all smaller than 0.2 m for 10-min prediction arc (the period of interruption of onboard observation is usually less than 10 min according to Fig. 4) and increase with increasing prediction time, which can be described in a linear expression. Thus, the position variances σ_i^2 in $\boldsymbol{P}_k^-$ can be set as $\sigma_i^2 = \sigma_0^2 + i \times d\sigma^2, i = 0, 1, 2, 3 \ldots$ considering the decrease of prediction accuracy with the increase of prediction arc. i is the ith epoch after the epoch when data recover. $(0.2\ \mathrm{m})^2$ is adopted for σ_0^2 as the position variance of the first epoch. $d\sigma^2$ is the decrease factor of the position variance and set to $(5\ \mathrm{cm})^2$ by experience. Meanwhile, the ambiguities are re-estimated after data recovered and the corresponding variances in $\boldsymbol{P}_k^-$ are set as $(60\ \mathrm{m})^2$.

Fig. 10 displays the flowchart of real-time PPP for LEO orbit determination. We add three new modules for real-time orbit determination: the interruption and jump detection module; the

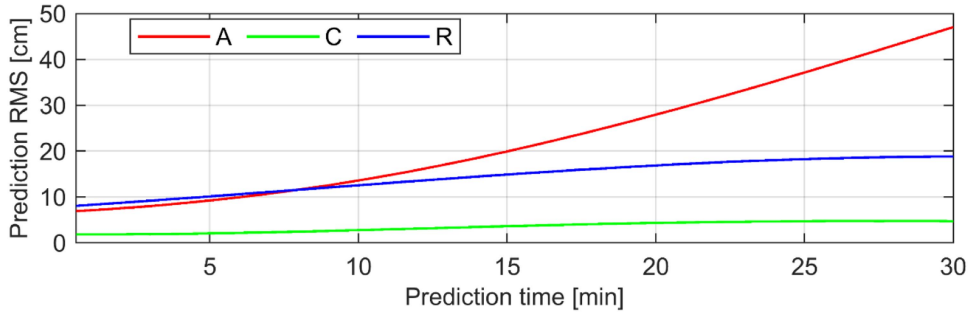

Fig. 9. Averaged RMSE values of prediction errors for 30 days in along-track (A), cross-track (C), and radial (R) directions within 30 min.

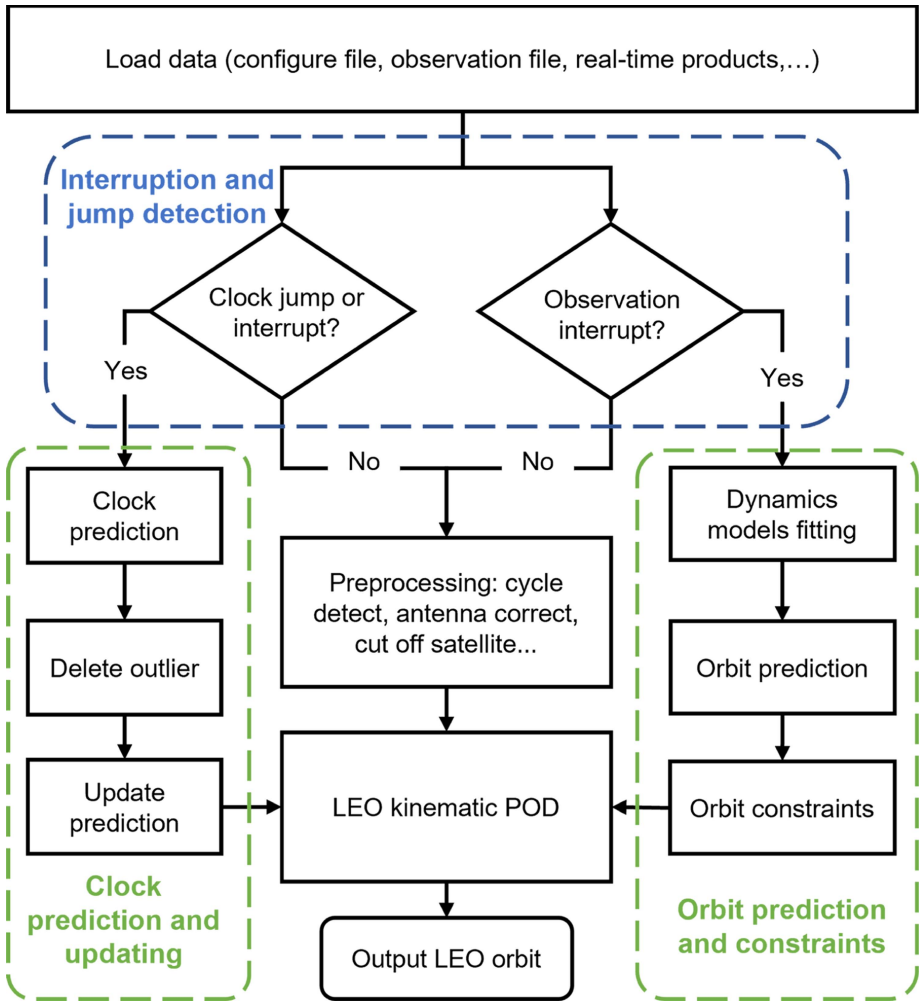

Fig. 10. Flow chart for LEO real-time KPOD. Dashed boxes indicate the three new modules, including the interruption and jump detection module, the CP and updating module, and the orbit prediction and constraints module.

CP and updating module; and the orbit prediction and constraints module. The first module is applied to detect clock jump and interruption as well as the interruption of onboard observations. When real-time clock is detected as abnormal, the second module is enabled to fix and replace outliers with predicted clock corrections for clock interruption and jump, respectively. The third module predicts orbit with dynamic models and applies OC for accelerating reconvergence when onboard observation interrupts.

IV. Results and Analysis

With the aforementioned method, one-month (January, 2019) real-time PPP for LEO POD is conducted. The reduced-dynamic

TABLE III
RMSE VALUES AND CORRESPONDING IMPROVEMENT FOR REAL-TIME PPP WITH AND WITHOUT (W/O) CP FOR GRACE-D FROM 01:15:50 TO 02:15:50 ON JANUARY 10, 2019

	Along-track		Cross-track		Radial	
	w/o CP	with CP	w/o CP	with CP	w/o CP	with CP
RMSE [cm]	9.57	5.26	17.04	2.33	19.33	6.00
Improvements [%]	45.03		86.33		68.96	

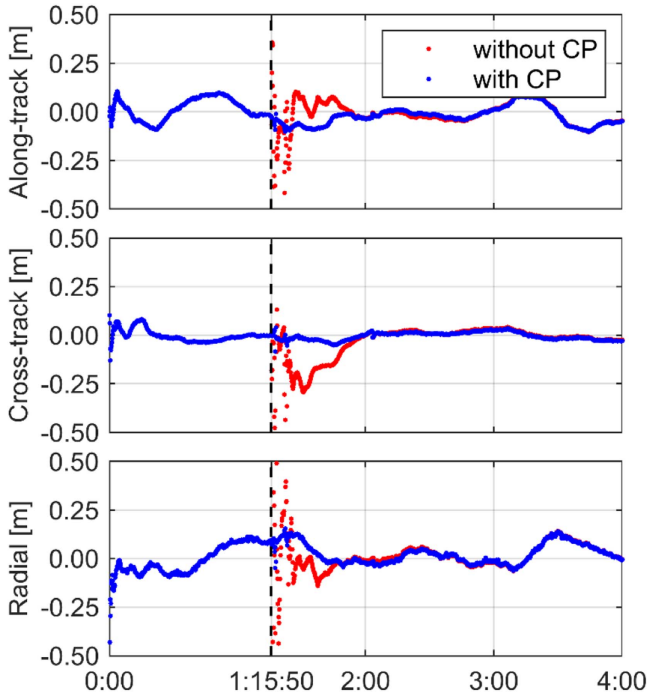

Fig. 11. Performance of real-time PPP for GRACE-D with (blue) and without (red) CP after clock interruption on January 10, 2019. Black dash line denotes the time when clock interruption occurs.

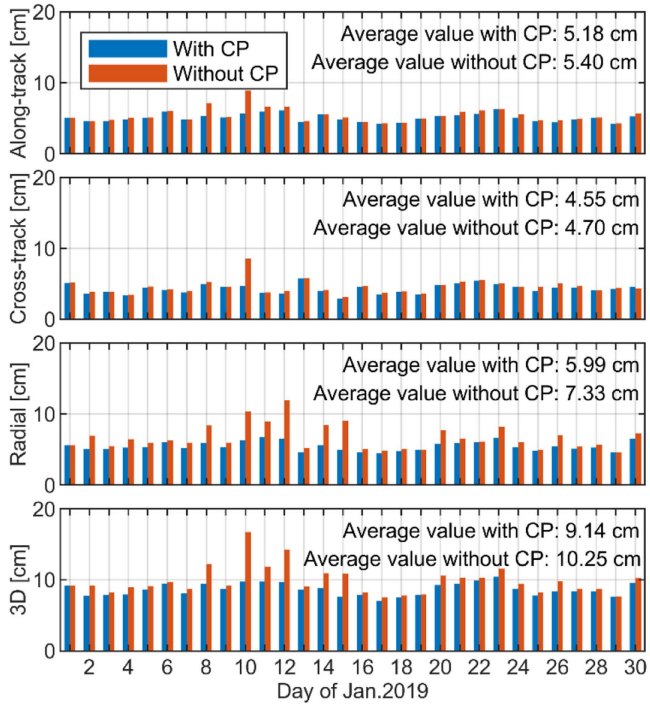

Fig. 12. Daily RMSE of position errors in along-track, cross-track, radial directions and 3D with (blue) and without (red) CP for GRACE-D in January, 2019. Averaged RMSE values are in the upper right corner of each subplot.

orbit from JPL (GNV1B data) is used as reference orbit and the convergence time is defined as the time when the positioning errors for each component reach $\pm$ 10 cm and stays within that value for at least 20 min.

Fig. 11 shows the real-time orbit errors in along-track, cross-track, and radial components with and without CP on January 10, 2019. It can be found that real-time PPP suffer from re-convergence from about 1:16 without CP while there is almost no reconvergence with CP. This is mainly caused by the clock interruption happened at 1:15:50 as shown in Fig. 1. At 1:15:50, the positioning errors without CP and by using broadcast clocks in along-track, cross-track, and radial components are -0.07, -0.18, and -0.98 m, respectively. With clock jump detection and prediction, broadcast clocks with large errors are detected and replaced by prediction values, making the positioning errors smaller than 0.1 m. During the interruption, the RMS values without CP in along-track, cross-track, and radial components are 0.25, 0.23, and 0.71 m, respectively, while that with CP are 0.05, 0.02, and 0.08 m, respectively. At the moment when clock corrections recovered, the positioning errors without CP and clock jump detection are still larger than 0.1 m, while those with CP and clock jump detection keep smaller than 0.1 m. Moreover, clock jumps often occur after real-time corrections recovered, which will introduce large errors into parameter estimation and lead to longer duration of reconvergence if the method of clock jump detection and CP is not adopted. With clock jump detection and prediction, the orbit quality shows great improvement when real-time GNSS clock interrupts, as indicated by the RMSE given in Table III. The RMSE for the kinematic orbits with CP in along-track, cross-track, and radial components are 5.26, 2.33, and 6.00 cm respectively, improved by 45.03%, 86.33%, and 68.96%.

Fig. 12 presents the daily RMSE of orbit with and without CP method in January, 2019. It can be found that the average RMSE of orbit in along-track, cross-track, and radial components are improved from 5.40, 4.70, and 7.33 cm to 5.18, 4.55, 5.99 cm, respectively. The 3-D RMSE is improved by 10.83%. These results confirm that the detection methods for clock jumps and interruptions are practical and the predicted clock corrections can effectively improve the orbit quality as well as avoiding PPP reconvergence in real-time LEO kinematic orbit determination.

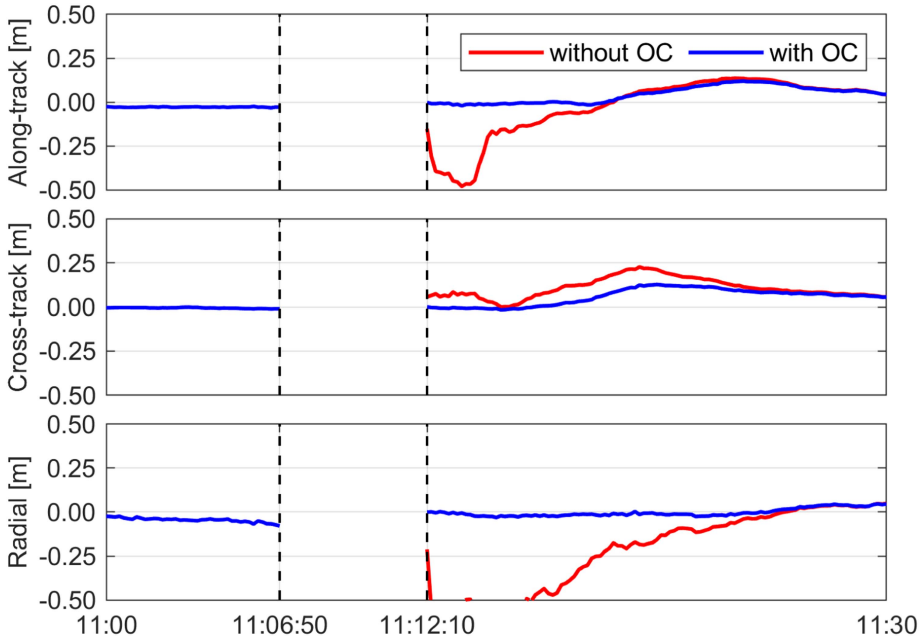

Fig. 13. Performance of real-time PPP for GRACE-D orbit with (blue) and without (red) OC after onboard observation interruption on January 26, 2019. Black dash lines denote the period of observation data interruption (from 11:06:50 to 11:12:10).

TABLE IV
RMSE VALUES AND CORRESPONDING IMPROVEMENT FOR REAL-TIME PPP WITH AND WITHOUT (W/O) OC FOR GRACE-D FROM 11:06:50 TO 12:06:50 ON JANUARY 26, 2019

	Along-track		Cross-track		Radial	
	w/o OC	With OC	w/o OC	With OC	w/o OC	With OC
Convergence time [min]	4.67	0.00	13.50	0.00	10.83	0.00
RMSE [cm]	9.77	4.33	8.14	6.22	19.37	3.60
Improvements [%]	55.68		23.58		82.26	

TABLE V
RMSE AND IMPROVEMENT OF REAL-TIME PPP WITH AND WITHOUT NEW METHOD FOR GRACE-C/D, JANUARY 1–30, 2019

	GRACE-C				GRACE-D			
RMSE [cm]	Along	Cross	Radial	3D	Along	Cross	Radial	3D
With CP and OC	5.47	3.95	5.82	8.91	5.14	4.37	5.52	8.72
w/o CP and OC	6.07	4.39	7.34	10.49	5.40	4.70	7.33	10.25
Improvement [%]	9.88	10.02	20.71	15.06	4.81	7.02	24.60	14.93

As for onboard observation interruption, Fig. 13 illustrates the performance of real-time PPP for GRACE-D with and without OC on January 26, 2019. It can be found that the orbit errors in radial and along-track directions exceed 0.5 m after the observation interruption without OC, while after applying OC, the orbit quality is greatly improved from 9.77, 8.14, and 19.37 cm to 4.33, 6.22, and 3.60 cm for along-track, cross-track, and radial directions, respectively as given in Table IV. The 3-D RMSE is reduced from 23.17 cm to 8.39 cm, representing an improvement of 63.79%. Moreover, there is even no reconvergence with OC while it takes about 14 minutes to reconverge without OC.

Table V gives the RMSE and improvement of real-time orbit determination with and without CP and OC for GRACE-C and GRACE-D in January, 2019. The averaged RMSE of GRACE-C orbit in along-track, cross-track, and radial components are improved from 6.07, 4.39, and 7.34 cm to 5.47, 3.95, and 5.82cm, respectively. Similarly, the average RMSE of GRACE-D orbit in the same components are reduced from 5.40, 4.70, and 7.32 cm to 5.14, 4.37, and 5.52 cm, respectively. The 3-D RMSE of both GRACE-FO satellites are smaller than 10 cm after the adoption of our proposed method, with an improvement of about 15%.

V. DISCUSSION AND CONCLUSION

With the promotion of LeGNSS and the increasing demand of real-time LEO services, real-time precise LEO orbits become particularly important. However, the jump and interruption of

real-time clock corrections as well as the LEO onboard observation interruption occur frequently, which would inevitably cause PPP reconvergence, leading to large orbit errors and threating the real-time LEO enhanced services and applications.

A new method of zero-reconvergence PPP for real-time LEO orbit determination in case of data interruption is put forward in order to shorten or even avoid reconvergence and improve the orbit quality as well. The method includes two aspects: one is that the orbit constraint with predicted orbit is put forward to accelerate the reconvergence caused by the interruption of onboard observation. The other is that the clock detection and prediction is applied to shorten the reconvergence on LEO satellites after the interruption of GNSS clock corrections. The performances of the method are comprehensively evaluated and the conclusions are as follow.

For the interruption of onboard observation data, orbit constraint is used in real-time KPOD. The results show that there is no reconvergence with orbit constrain while more than 10 min is needed after the onboard observations recovered. Moreover, the accuracy of real-time LEO orbit in along-track, cross-track, and radial components are reduced from 9.77, 8.14, and 19.37 cm to 4.33, 6.22, and 3.60 cm with orbit constrain. Actually, the accuracy of the predicted LEO orbit is the key to apply orbit constraint since it determines not only the effectiveness in shortening reconvergence time, but also how long the interruption duration that the method can handle. If the predicted orbit can achieve centimeter-level accuracy within one-hour prediction, then zero-reconvergence can be obtained even when the duration of onboard data interruption lasts one hour.

For the jump and interruption of real-time GNSS clock corrections, clock jump detection and Chebyshev extrapolation are applied. The results show that the CP would effectively provide reliable real-time clock corrections and improve the orbit accuracy from 5.4, 4.7, and 7.33 cm to 5.18, 4.55, and 5.99 cm in along-track, cross-track, and radial directions, respectively. In addition, the CP can shorten the convergence time or even realize zero-reconvergence when real-time clock interruption occurs.

The above results verify the feasibility and performance of the zero-reconvergence PPP for LEO orbit determination in case of data interruption. It is promising that the method would provide real-time precise LEO orbit and guarantee the normal operation of real-time LEO enhanced services and applications in the near future.

REFERENCES

[1] T. H. Xu and Y. X. Yang, "CHAMP gravity field recovery using kinematic orbits," *Chin. J. Geophys.*, vol. 48, no. 2, pp. 319–325, 2005.

[2] T. Mayer-Gürr, R. Savcenko, W. Bosch, I. Daras, F. Flechtner, and C. Dahle, "Ocean tides from satellite altimetry and GRACE," *J. Geodyn.*, vol. 59/60, pp. 28–38, 2012.

[3] Q. Xiao, X. Geng, J. Chen, L. Meng, N. Li, and Y. Zhang, "Calibration methods of the interference magnetic field for low earth orbit (LEO) magnetic satellite," *Acta Geologica Sinica*, vol. 61, pp. 3134–3138, Aug. 2018.

[4] D. Švehla and M. Rothacher, "Kinematic and reduced-dynamic precise orbit determination of low earth orbiters," *Adv. Geosci.*, vol. 1, pp. 47–56, 2003.

[5] T. P. Yunck, S. - C. Wu, J. - T. Wu, and C. L. Thornton, "Precise tracking of remote sensing satellites with the global positioning system," *IEEE Trans. Geosci. Remote Sens.*, vol. 28, no. 1, pp. 108–116, Jan. 1990, doi: 10.1109/36.45753.

[6] A. Jäggi, R. Dach, O. Montenbruck, U. Hugentobler, H. Bock, and G. Beutler, "Phase center modeling for LEO GPS receiver antennas and its impact on precise orbit determination," *J. Geodesy*, vol. 83, no. 12, pp. 1145–1162, Dec. 2009.

[7] T. G. Reid, A. M. Neish, T. F. Walter, and P. K. Enge, "Leveraging commercial broadband LEO constellations for navigating," in *Proc. 29th Int. Tech. Meeting Satell. Division Inst. Navig.*, 2016, pp. 2300–2314.

[8] S. Malys and P. A. Jensen, "Geodetic point positioning with GPS carrier beat phase data from the CASA UNO experiment," *Geophys. Res. Lett.*, vol. 17, no. 5, pp. 651–654, 1990.

[9] J. F. Zumberge, M. B. Heflin, D. C. Jefferson, M. M. Watkins, and F. H. Webb, "Precise point positioning for the efficient and robust analysis of GPS data from large networks," *J. Geophys. Res. Solid Earth*, vol. 102, no. B3, pp. 5005–5017, 1997.

[10] O. Montenbruck, "Kinematic GPS positioning of LEO satellites using ionosphere-free single frequency measurements," *Aerosp. Sci. Technol.*, vol. 7, no. 5, pp. 396–405, 2003.

[11] D. Švehla and M. Rothacher, "Kinematic positioning of LEO and GPS satellites and IGS stations on the ground," *Adv. Space Res.*, vol. 36, no. 3, pp. 376–381, 2005.

[12] H. Bock, A. Jäggi, D. Švehla, G. Beutler, U. Hugentobler, and P. Visser, "Precise orbit determination for the GOCE satellite using GPS," *Adv. Space Res.*, vol. 39, no. 10, pp. 1638–1647, 2007.

[13] N. Zehentner and T. Mayer-Gürr, "Precise orbit determination based on raw GPS measurements," *J. Geodesy*, vol. 90, no. 3, pp. 275–286, Mar. 2016.

[14] H. Ge, B. Li, L. Nie, M. Ge, and H. Schuh, "LEO constellation optimization for LEO enhanced global navigation satellite system (LeGNSS)," *Adv. Space Res.*, vol. 66, no. 3, pp. 520–532, 2020.

[15] M. Caissy, L. Agrotis, G. Weber, M. Pajares, and U. Hugentobler, "The international GNSS real-time service," *GPS World*, vol. 23, pp. 52–58, Jun. 2012.

[16] T. Hadas and J. Bosy, "IGS RTS precise orbits and clocks verification and quality degradation over time," *GPS Solutions*, vol. 19, no. 1, pp. 93–105, Jan. 2015.

[17] B. Li, H. Ge, Y. Bu, Y. Zheng, and L. Yuan, "Comprehensive assessment of real-time precise products from IGS analysis centers," *Satell. Navig.*, vol. 3, no. 1, Jun. 2022, Art. no. 12.

[18] P. Chen, J. Zhang, and X. Sun, "Real-time kinematic positioning of LEO satellites using a single-frequency GPS receiver," *GPS Solutions*, vol. 21, no. 3, pp. 973–984, Jul. 2017.

[19] X. Li, J. Wu, K. Zhang, X. Li, Y. Xiong, and Q. Zhang, "Real-time kinematic precise orbit determination for LEO satellites using zero-differenced ambiguity resolution," *Remote Sens.*, vol. 11, no. 23, 2019, Art. no. 25120.

[20] Z. Wang et al., "Comparison of the real-time precise orbit determination for LEO between kinematic and reduced-dynamic modes," *Measurement*, vol. 187, 2022, Art. no. 110224.

[21] Z. Wang et al., "Real-time precise orbit determination for LEO between kinematic and reduced-dynamic with ambiguity resolution," *Aerospace*, vol. 9, no. 1, 2022, Art. no. 25460.

[22] K. Wang, J. Liu, H. Su, A. El-Mowafy, and X. Yang, "Real-time LEO satellite orbits based on batch least-squares orbit determination with short-term orbit prediction," *Remote Sens.*, vol. 15, no. 1, 2023, Art. no. 133.

[23] A. El-Mowafy, M. Deo, and N. Kubo, "Maintaining real-time precise point positioning during outages of orbit and clock corrections," *GPS Solutions*, vol. 21, no. 3, pp. 937–947, Jul. 2017.

[24] L. Zhang, H. Yang, Y. Yao, Y. Gao, and C. Xu, "A new datum jump detection and mitigation method of real-time service (RTS) clock products," *GPS Solutions*, vol. 23, no. 3, May 2019, Art. no. 67.

[25] G. Busca and Q. Wang, "Time prediction accuracy for a space clock," *Metrologia*, vol. 40, no. 3, Jun. 2003, Art. no. S265.

[26] Z. Zheng, X. Lu, and Y. Chen, "Improved grey model and application in real-time GPS satellite clock bias prediction," in *Proc. 4th Int. Conf. Natural Comput.*, 2008, pp. 419–423.

[27] Y. Wang, Z. Lu, D. Sun, and N. Wang, "A new navigation satellite clock bias prediction method based on modified clock-bias quadratic polynomial model," *ACTA Astronomica Sinica*, vol. 57, no. 1, pp. 78–90, 2016.

[28] H. Yang, Y. Gao, L. Zhang, and Z. Nie, "A new satellite clock offsets prediction method based on the IGS RTS products," in *Proc. China Satell. Navig. Conf.*, 2018, pp. 251–264.

[29] Z. Nie, Y. Gao, Z. Wang, S. Ji, and H. Yang, "An approach to GPS clock prediction for real-time PPP during outages of RTS stream," *GPS Solutions*, vol. 22, no. 1, Nov. 2017, Art. no. 14.

[30] V. Sreeja, M. Aquino, Z. G. Elmas, and B. Forte, "Correlation analysis between ionospheric scintillation levels and receiver tracking performance," *Space Weather*, vol. 10, no. 6, 2012, Art. no. 2530.
[31] R. K. Crane, "Ionospheric scintillation," *Proc. IEEE*, vol. 65, no. 2, pp. 180–199, Feb. 1977, doi: 10.1109/PROC.1977.10456.
[32] K. Guo, M. Aquino, and S. Vadakke Veettil, "Ionospheric scintillation intensity fading characteristics and GPS receiver tracking performance at low latitudes," *GPS Solutions*, vol. 23, no. 2, Feb. 2019, Art. no. 43.
[33] H. Zhang, Y. Yuan, W. Li, B. Zhang, and J. Ou, "A grid-based tropospheric product for China using a GNSS network," *J. Geodesy*, no. 92, pp. 765–777, 2018.
[34] X. Ren, J. Chen, X. Li, X. Zhang, and F. Mohamed, "Performance evaluation of real-time global ionospheric maps provided by different IGS analysis centers," *GPS Solutions*, vol. 23, no. 4, 2019, Art. no. 25460.
[35] D. A. Vallado and W. D. McClain, *Fundamentals of Astrodynamics and Applications*, 4th ed., Hawthorne, CA, USA: Microcosm Press, 2013.
[36] B. Li, N. Zang, H. Ge, and Y. Shen, "Single-frequency PPP models: Analytical and numerical comparison," *GPS Solutions*, vol. 93, no. 12, pp. 2499–2514, Dec. 2019.
[37] P. Rebischung and R. Schmid, "IGS14/igs14.atx: A new framework for the IGS products," in *Proc. AGU Fall Meeting Abstr.*, 2016, pp. G41A–0998.
[38] *Gravity Recovery and Climate Experiment Follow-On (GRACE-FO) Level-1 Data Product User Handbook*. New York, NY, USA: JPL, 2019.
[39] J. T. Wu, S. C. Wu, G. A. Hajj, W. I. Bertiger, and S. M. Lichten, "Effects of antenna orientation on GPS carrier phase," *Astrodynamics*, vol. 31, pp. 1647–1660, Aug. 1992.
[40] Y. Lv, Z. Dai, Q. Zhao, S. Yang, J. Zhou, and J. Liu, "Improved short-term clock prediction method for real-time positioning," *Sensors*, vol. 17, no. 6, 2017, Art. no. 23560.
[41] H. Ge, B. Li, T. Wu, and S. Jiang, "Prediction models of GNSS satellite clock errors: Evaluation and application in PPP," *Adv. Space Res.*, vol. 68, no. 6, pp. 2470–2487, 2021.
[42] X. Liu, X. Wu, Y. Tian, and Y. Deng, "Study on atomic prediction of time based on interpolation model with tchebytchev polynomiais," *J. Geodesy Geodyn.*, vol. 30, no. 1, 2010, Art. no. 77.
[43] X. Wang, "The analysis and comparision of clock error prediction models," *GNSS World China*, vol. 43, no. 2, pp. 84–90, 2018.
[44] R. Kalman, "A new approach to linear filtering and prediction problems," *J. Fluids Eng.*, vol. 82, no. 1, pp. 35–45, 1960.
[45] J. Woods and C. Radewan, "Kalman filtering in two dimensions," *IEEE Trans. Inf. Theory*, vol. 23, no. 4, pp. 473–482, Jul. 1977.
[46] R. Zhang and G. Liu, "Discussion on orbit fitting and orbit forecasting of low earth orbit satellites," *J. Geodesy Geodyn.*, vol. 28, no. 4, pp. 115–120, 2008.
[47] H. Ge, B. Li, M. Ge, L. Nie, and H. Schuh, "Improving low earth orbit (LEO) prediction with accelerometer data," *Remote Sens.*, vol. 12, no. 10, 2020, Art. no. 2540.
[48] C. He et al., "Impact of thermospheric mass density on the orbit prediction of LEO satellites," *Space Weather*, vol. 18, no. 1, 2020, Art. no. e2019SW002336.
[49] K. Wang, A. El-Mowafy, and X. Yang, "URE and URA for predicted LEO satellite orbits at different altitudes," *Adv. Space Res.*, vol. 70, no. 8, pp. 2412–2423, 2022.
[50] Y. Wang, S. Zhong, H. Tao, and J. Ou, "Precision analysis of LEO satellite orbit prediction," *Acta Geodaetica et Cartographica Sinica*, vol. 45, no. 9, pp. 1035–1041, 2016.
[51] C. Foerste et al., "A new release of EIGEN-6: The latest combined global gravity field model including LAGEOS, GRACE and GOCE data from the collaboration of GFZ Potsdam and GRGS Toulouse," in *Proc. EGU Gen. Assem. Conf. Abstr.*, 2012, pp. 2821.
[52] G. Petit and B. Luzum, "IERS conventions (2010)," *Tech. Rep. DTIC Document*, vol. 36, Jan. 2010, Art. no. 180.
[53] R. Savcenko and W. Bosch, "EOT11A - empirical ocean tide model from multi-mission satellite altimetry," Deutsches Geodtisches Forschungsinstitut, München, Germany, Tech. Rep. 89, 2008.
[54] S. Bettadpur, "GRACE product specification document," Center for Space Research, Univ. Texas Austin, Austin, TX, USA, Tech. Rep. CSR-GR-03-02, v4.6, 2012.
[55] C. Berger, R. Biancale, M. Ill, and F. Barlier, "Improvement of the empirical thermospheric model DTM: DTM94 – a comparative review of various temporal variations and prospects in space geodesy applications," *J. Geodesy*, vol. 72, no. 3, pp. 161–178, Mar. 1998.
[56] E. M. Standish, "JPL planetary and lunar ephemerides," Interoffice Memorandum, Los Angeles, CA, USA, Tech. Rep. DE405/LE405, 1998.

Haibo Ge received the B.Sc. degree in surveying and mapping engineering, and the Ph.D. degree in surveying and mapping from Tongji University, Shanghai, China, in 2013 and 2018, respectively.

He is currently an Assistant Professor with Tongji University. His research interest is precise orbit determination and positioning for LEO-enhanced GNSS.

Guanlong Meng is working toward the M.S. degree in surveying and mapping in Tongji University, Shanghai, China.

His major research orientation is precise orbit determination of LEO satellites.

Bofeng Li received the B.Sc. degree in surveying and mapping engineering, and the Ph.D. degree in geodesy and survey engineering from Tongji University, Shanghai, China, in 2005 and 2010, respectively.

He is currently a Professor in geodesy with Tongji University, Shanghai, China. His research interests include GNSS ambiguity resolution and precise positioning, precise orbit determination, and multisensor integrated seamless positioning.